Ionization waves in electron-beam-assisted, shielded capillary discharge

I. Rutkevich, M. Mond, and Y. Kaufman*
Department of Mechanical Engineering, Ben-Gurion University, Beer Sheva 84105, Israel

P. Choi
LPMI, Ecole Polytechnique, 91128 Palaiseau, France

M. Favre
Facultad de Física, Pontificia Universidad Católica de Chile, Casilla 306, Santiago 22, Chile
(Received 10 February 2000)

A theory of propagation of cathode-directed ionization waves during the early stages of an electrical breakdown in a shielded, low-pressure capillary is developed. The discharge process occurs due to the ionization of the low-density gas in the capillary by an electron beam that is emanating from a hollow cathode. Due to the strong electric field in the capillary the electrons are in the fast acceleration regime. Consequently, the full momentum equation for the electrons is employed, rather than the electron drift velocity approach. The smallness of the ratio of the capillary radius to the characteristic length of the electric potential variation in the axial direction allows the construction of a quasi-one-dimensional model. The latter retains the important two-dimensional nature of the electron flow as well as the electrodynamic boundary conditions at the capillary wall and the conducting shield and results in a set of one-dimensional, time-dependent partial differential equations for the on-axis distributions of the physical quantities. It is shown that those equations admit self-similar solutions that represent ionization waves propagating with constant velocities. The resulting set of ordinary differential equations is solved numerically for various initial conditions representing a nonperturbed steady state ahead of the ionization front and the resulting features of the ionization waves are investigated and discussed. The obtained solutions describe both ionization growth and virtual anode propagation and represent fast ionization waves in plasma waveguides, for which the maximum value of the mean electron velocity is much higher than the wave velocity. The space-charge distribution associated with the ionization waves is found in the form of plasma oscillations with a continuously increasing frequency and a solitary envelope. The calculated wave velocity increases with the gas pressure and this tendency is in agreement with corresponding experimental observations.

PACS number(s): 52.35.Mw, 52.25.Jm, 52.75.Kq

I. INTRODUCTION AND BACKGROUND

Long-term experimental studies of electrical breakdown of gas-filled discharge gaps have shown that in many cases the ionization growth starts with the propagation of ionization waves (IWs). IWs are observed in shielded discharge tubes with a large length-to-radius ratio [1–5] as well as in planar gaps between parallel electrodes. For various experimental conditions two different kinds of IWs may be observed in planar discharge gaps, quasiplanar IWs that are weakly nonuniform in directions parallel to the electrode walls [6,7] and streamers representing highly nonuniform filaments oriented parallel to the applied electric field and growing rapidly in both anode and cathode directions [8,9]. Most of the theoretical models describing the propagation of quasiplanar IWs [10,11], IWs in long discharge tubes [11], and streamers [12,13] use the local-field approximation which allows calculating the mean ionization frequency and the mean electron velocity as functions of the local electric field.

The local-field approximation, which is appropriate for a wide range of parameters of pulse discharge at moderate and high pressures, becomes invalid for low-pressure discharge ($p<1$ Torr) at sufficiently high values of the electric field-to-gas density ratio E/N. Thus, the experiments with transient hollow cathode discharge [14,15] and hollow-cathode-assisted capillary discharge [16,17] deal with such high values of E/N, for which neither the Townsend ionization coefficient nor the electron drift velocity approach can be used. Both kinds of low-pressure discharge mentioned above admit propagation of IWs at the prebreakdown stage, which are stimulated by an electron beam injected to the anode-cathode gap from the cathode hole. The modeling of such IWs is important for determining the time delay of the electrical breakdown and for a better understanding of the transition to a high-current stage of the discharge resulting in the creation of a hot, fully ionized plasma.

The objective of the present paper is to develop a model for the propagation of cathode-directed IWs and to examine its relation to the concept of virtual anode propagation in an electron-beam-assisted fast capillary discharge (FCD), whose total operation time is in the range 10–100 ns. Such a discharge can be used in various applications as a high brightness source of vacuum-ultraviolet and soft-x-ray emission. To achieve fast formation of the discharge plasma, the initial on-axis ionization path is prepared through the transient hollow cathode effect [16,17].

*Present address: Physics Department, NRCN, POB 9001, Beer Sheva, Israel.

 ©2000 The American Physical Society

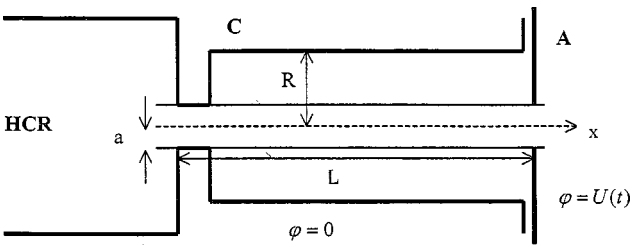

FIG. 1. Sketch of a shielded capillary discharge: *A*, anode; *C*, cathode; HCR, hollow cathode region; *a*, the capillary radius; *L*, the capillary length; *R*, the shield radius.

We consider the process of ionization growth leading to an electrical breakdown of a hollow-cathode-assisted capillary that represents a narrow discharge tube $0<x<L, 0<r<a$ with the large aspect ratio $(L/a \gg 1)$. The capillary is filled with a low-pressure electropositive gas with initial particle density $N_0(x)$. The ends of the capillary $x=0$ and $x=L$ are inserted into the gas-filled hollow cathode and hollow anode cavities, respectively. With the exception of a short near-anode part, the discharge tube is surrounded by a conducting shield $r=a+h(x)$ having the cathode potential $(\varphi=0)$ as is shown in Fig. 1. The anode potential is considered as a given function of time $U(t)$. The region $a<r<R(x)=a+h(x)$ is filled with a dielectric medium with a given dielectric permittivity ε. If the capillary wall material differs from the dielectric spacer between the outer wall of a tube and the conducting shield then such a two-layered dielectric shell will be characterized by the effective permittivity $\varepsilon_{\text{eff}}=\varepsilon(x)$. The discharge is assumed to be axially symmetric: in cylindrical coordinates the electric field as well as the parameters of the discharge plasma does not depend on the azimuth angle.

The expected scenario of the ionization growth in a FCD is as follows. When a high-voltage pulse is applied to the anode, it creates an inhomogeneous electric field **E** in the gas and in the dielectric region. At the instant when the anode potential reaches its maximum value, the electric field in a gaseous medium is maximal in the region which is close to the anode end of the capillary and decreases to the cathode end due to the presence of the conducting shield.

If the gas in the capillary is not initially ionized but some amount of initial electrons is produced by triggering the hollow cathode, as was done in experiments [16,17], the ionization by the electron-atom impact begins in the hollow cathode region (HCR). The electrons created in the HCR move to the cathode hole and enter into the capillary where they undergo fast acceleration by a strong electric field and transition to the runaway regime. The ionization by a fast electron beam in the capillary results in the creation of positive space charge in the near-anode domain since the fast electrons are moving to the anode, while the relatively slow ions remain close to the place of their birth. The space charge is growing in the direction to the anode and after some time this leads to the screening of the electric field near the anode and to the shift of the field maximum closer to the cathode end. This is the stage of propagation of IWs transferring the anode potential to the cathode hole. The structure of IWs may contain plasma oscillations, whose frequency increases across the wave due to continuous ionization growth.

When the ionization front reaches the cathode hole, the plasma behind the IWs is not yet fully ionized. The distributions of the electric field and the electron and ion densities at this instant can be used as initial conditions for the modeling of further stages of the capillary discharge evolution, including the transition to full ionization, the rapid increase of the total electric current, the discharge constriction by ponderomotive force (micro-*z* pinch), the creation of multicharged ions, and soft-x-ray emission.

The HCR is characterized by relatively low values of the ratio E/N, for which the local-field approximation can be employed for calculating the mean (drift) electron velocity and the ratio of the ionization frequency to the concentration of neutral atoms ν_i/N that can be considered as given functions of E/N [18,19]. Unlike the HCR where the electric field is much less than the average axial field in the capillary $E_U=U/L$, the capillary domain is characterized by large values of E/N which provide very fast acceleration of near-axis electrons. This situation is similar to the electron runaway that was considered for fully ionized plasma in [20] and was observed also in high-overvoltage electric breakdown when the plasma is weakly ionized and the electron-neutral atom collisions dominate [7]. In the presence of fast electrons the electron drift velocity approach as well as the local-field approximation for the ionization rate cannot be used for the modeling of ionization growth in the capillary. Here we meet conditions when the inertial term in the momentum equation for electrons must be taken into account and the ionization occurs mainly due to collisions of the fast electrons with the atoms in the ground state.

The paper is organized as follows: In Sec. II the ionization source and the effective friction force due to elastic and ionizing electron-atom collisions are derived with the aid of the Boltzmann equation for electrons. When calculating the integrals in the velocity space representing the source and friction terms, the approximation of a monoenergetic beam is used for the electron distribution function. In Sec. III a system of quasi-one-dimensional (Q1D) macroscopic equations for determining the on-axis distributions of the plasma parameters and the on-axis electric potential is obtained. It is shown that the electron velocity can be approximated as a potential field. A complete Q1D description is achieved by introducing the radial profiles of the electric potential and of the electron velocity potential and by using the electrodynamic boundary conditions at the plasma-dielectric wall interface and at the conducting shield. In Sec. IV numerical solutions of the Q1D equations in the form of steady-state cathode-directed waves propagating with constant velocity are presented. The wave velocity has been found to be an increasing function of the gas pressure. It has been shown that the obtained solutions describe both the ionization wave and virtual anode propagation and represent fast IWs in plasma waveguides, for which the maximum value of the mean electron velocity is much higher than the wave velocity. The space-charge distribution associated with the IW represents plasma oscillations characterized by a continuously increasing Langmuir frequency with a solitary envelope. The main results are discussed in Sec. V.

II. BEAM APPROXIMATION FOR THE IONIZATION SOURCE AND EFFECTIVE FRICTION

The macroscopic equations describing the ionization growth in the capillary at the prebreakdown stage include the rate equation for electrons

$$\frac{\partial n_e}{\partial t} + \mathrm{div}(n_e \mathbf{V}) = S \tag{1}$$

and for single-charged positive ions

$$\frac{\partial n_i}{\partial t} = S. \tag{2}$$

Here n_e and n_i are the concentrations of electrons and ions, respectively, $\mathbf{V}$ is the mean electron velocity, and S is the ionization source, which can be presented in the form

$$S = \overline{\nu_i} n_e,$$

$$\overline{\nu_i} = \int_{|\mathbf{w}| = \sqrt{2I/m}}^{\infty} \nu_i(K) \overline{f}(\mathbf{w}, \mathbf{r}, t) d\mathbf{w}, \tag{3}$$

$$\nu_i(K) = N \Sigma_i(K) \sqrt{2K/m}.$$

In Eq. (3) ν_i is the ionization frequency, I is the first ionization potential, m is the electron mass, $\mathbf{w}$ and $K = mw^2/2$ are the random values of the electron velocity and the kinetic energy, respectively, $\Sigma_i = \Sigma_i(K)$ is the ionization cross section, and $\overline{f} = f/n_e$ is the normalized electron distribution function, i.e., the integral of $\overline{f}$ over the whole velocity space equals one. For complex atoms Eq. (3) takes into account only direct ionization from the outer shell. Direct ionization from inner shells contributes to the ionization frequency in a similar way: the single integral in Eq. (3) is replaced by the sum of integrals containing the ionization potentials I_s and the ionization cross section Σ_{is} for various shells. The mean ion velocity is neglected in Eq. (2) since it is much less than the electron velocity V and the ionization wave velocity W and thus the contribution of the ion motion to the electric current density is small. The form of the source term (3) reflects the fact that the dominant process determining the ionization growth at the prebreakdown stage of the capillary discharge is direct ionization of atoms in the ground state by electron impact. The indirect (step) ionization is neglected due to relatively low populations of excited atomic levels. Recombination is also neglected since the characteristic time of ionization growth is much shorter than the time needed to achieve ionization equilibrium.

Taking into account the inertial term in the electron momentum equation is necessary when the electrostatic force eE is much larger than the dynamic friction F provided by the mean loss of momentum μ of an electron in the field direction due to elastic and inelastic collisions of electrons with atoms. This condition is fulfilled if

$$E/N \gg K \Sigma_m(K)/|e|, \tag{4}$$

where Σ_m is the total cross section of the momentum transfer in electron-atom collisions, $e<0$ is the electron charge. Inequality (4) means that the characteristic time of the electron acceleration by the electric field is much less than the characteristic time of the electron-atom collisions. The experimental data for the total cross section of the electron-atom collisions in argon, including elastic scattering, ionizing collisions, and excitation of atomic levels [21,22] indicate that for $K<10$ keV the right-hand side of Eq. (4) does not exceed 3×10^{-13} V cm^2. Therefore, for a rarefied gas with the atomic density N of the order of 10^{16} cm^{-3} an electric field E of the order of 10 kV/cm is large enough to provide fast acceleration of the near-axis electrons. This is confirmed by the results of numerical simulation of IWs presented in Sec. IV.

To take into account the loss of energy and momentum of the electron gas in the complete range of energies that are responsible for ionizing collisions ($K>I$), the following approach is employed. The macroscopic momentum equation for the gas of electrons in the axial direction on the axis ($r=0$) is presented in the form

$$\frac{\partial (n_{e0} u)}{\partial t} + \mathrm{div}(n_e u \mathbf{V})_{r=0} = \frac{eE_0 n_{e0} - (F_{\mathrm{inel}} + F_{\mathrm{el}}) n_{e0}}{m}. \tag{5}$$

Here $n_{e0} = n_e(x, r=0, t)$ is the concentration of electrons on the axis, $E_0 = E_x(x, r=0, t)$ and $u = V_x(x, r=0, t)$ are the electric field and the mean electron velocity on the axis, respectively, F_{inel} and F_{el} are the effective friction forces provided by inelastic and elastic electron-atom collisions, respectively. The friction force due to electron-ion collisions is not included in Eq. (5) since the expected ionization degree at the prebreakdown stage of FCD is small, while the energies of electrons are large. These circumstances result in relatively low effective frequency of the Coulomb collisions. The electron momentum equation (5) can be obtained from the Boltzmann equation for the electron distribution function $f(\mathbf{w}, x, r, t)$, in which the terms representing both elastic and inelastic electron-atom collisions are taken into account

$$\frac{\partial f}{\partial t} + \mathbf{w} \cdot \nabla f + \frac{e\mathbf{E}}{m} \cdot \frac{\partial f}{\partial \mathbf{w}} = C_{\mathrm{el}}(f) + C_{\mathrm{inel}}(f), \tag{6}$$

where $C_{\mathrm{el}}(f)$ and $C_{\mathrm{inel}}(f)$ are operators of elastic and inelastic collisions; both are linear in f. The operator C_{el} is the Boltzmann collision integral, in which the Maxwellian distribution function for the atoms $f_a(\mathbf{w}_a)$ is assumed [23],

$$C_{\mathrm{el}}(f) = \int\int [f(\mathbf{w}') f_a(\mathbf{w}_a') - f(\mathbf{w}) f_a(\mathbf{w}_a)] \times |\mathbf{w} - \mathbf{w}_a| \Sigma_d(|\mathbf{w} - \mathbf{w}_a|, \chi) d\Omega \, d\mathbf{w}_a, \tag{7}$$

where $\mathbf{w}$ and $\mathbf{w}'$ are the velocities of the electron, $\mathbf{w}_a$ and $\mathbf{w}_a'$ are the velocities of the atom before and after the electron-atom collision, respectively, χ is the angle between the vectors $\mathbf{w} - \mathbf{w}_a$ and $\mathbf{w}' - \mathbf{w}_a'$, Σ_d is the differential cross section of the electron scattering by atoms, $d\Omega = 2\pi \sin\chi d\chi$ is the solid angle corresponding to the interval of scattering $(\chi, \chi + d\chi)$. For the sake of brevity the radius vector $\mathbf{r}$ and the time t are not shown in Eq. (7) as additional arguments of all distribution functions. The operator of inelastic collisions can be presented as follows:

$$C_{\mathrm{inel}}(f) = C_{\mathrm{inel}}^{-}(f) + C_{\mathrm{inel}}^{+}(f). \tag{8}$$

Here $-C_{\mathrm{inel}}^{-}(f) d\mathbf{w}$ is the density rate of electrons in the random velocity space $\mathbf{w}$ which leaves the volume $d\mathbf{w}$ due to excitation and ionization. For this term a simple relaxation-type model can be used [24]

$$C_{\rm inel}^{-}(f)=-\nu^{*}(w)f \quad (w=|\mathbf{w}|). \tag{9}$$

Here $\nu^{*}(w)$ is the total frequency of the electron energy loss by inelastic collisions and, therefore, it depends on the cross sections of ionization and excitations of electronic levels corresponding to discrete atomic states. The quantity $\nu^{*}(w)$ is zero for $K<I_{12}$ where I_{12} is the energy of the first excitation level. The quantity $C_{\rm inel}^{+}(f)d\mathbf{w}$ is the density rate of the electrons that appear in a small volume $d\mathbf{w}$ of the velocity space due to inelastic collisions. Neglecting the energy of such new free electrons in comparison with the energy of fast incident electrons, we present the term $C_{\rm inel}^{+}(f)$ as

$$C_{\rm inel}^{+}(f)=(\overline{\nu_i}+\overline{\nu^{*}})n_e\delta(\mathbf{w}),$$

$$\overline{\nu^{*}}n_e=\int_{|\mathbf{w}|>\sqrt{2I_{12}/m}}\nu^{*}(w)f(\mathbf{w},\mathbf{r},t)d\mathbf{w}. \tag{10}$$

Here $\overline{\nu_i}$ is the mean ionization frequency defined in Eq. (3) and $\delta(\mathbf{w})$ is the Dirac delta function. The form of the inelastic collision operators assumed in Eqs. (9) and (10) allows us to obtain the electron rate equation (1) by integrating the Boltzmann equation (6) over the whole velocity space: the integral of $C_{\rm inel}^{-}$ is canceled by the integral of the second term in $C_{\rm inel}^{+}$, while the integral of the term $C_{\rm el}$ always results in zero. The electron momentum equation is obtained by multiplying Eq. (6) by the random momentum $m\mathbf{w}$ and integrating over the velocity space. Then the term $m\mathbf{w}C_{\rm inel}^{+}(f)$ will not contribute to the mean momentum of the electron gas and the friction terms in Eq. (5) will be presented as

$$\frac{F_{\rm el}n_{e0}}{m}=-\int w_x C_{\rm el}[f(\mathbf{w},x,r=0,t)]d\mathbf{w},$$

$$\frac{F_{\rm inel}n_{e0}}{m}=\int_{|\mathbf{w}|>\sqrt{2I_{12}/m}}w_x\nu^{*}(w)f(\mathbf{w},x,r=0,t)d\mathbf{w}. \tag{11}$$

Since at the prebreakdown stage of the evolution of FCD the electrostatic force is much larger than the total friction, the mean electron trajectories are weakly perturbed by collisions, and a beamlike electron distribution function can be used for calculating the integrals representing such characteristics of the electron gas as the mean ionization frequency and the mean friction force. Calculating the integrals in Eq. (3) and in the second of Eqs. (11) with

$$f(\mathbf{w},\mathbf{r},t)=n_e(\mathbf{r},t)\,\delta(\mathbf{w}-\mathbf{V}(\mathbf{r},t)) \tag{12}$$

results in the following formulas for the mean ionization frequency $\overline{\nu_{i0}}$ on the axis:

$$\overline{\nu_{i0}}=Nu\Sigma_i(K_u), \quad K_u=mu^2/2 \tag{13}$$

and for the inelastic force

$$F_{\rm inel}/m=u\,\nu^{*}(|u|). \tag{14}$$

To obtain an expression for the inelastic part of the friction force that could be used in the range $K_u>I$ we start with the model in which only one type of inelastic collision is taken into account, namely, the ionization from the outer electronic shell of the atom by an electron impact. Assuming the beamlike form (12) for the electron distribution function, we can derive a simple relation between the values $\overline{\nu_{i0}}$ and $F_{\rm inel}/m$. Since the rate of the electron energy loss by ionization at $r=0$ should be equal to $I\overline{\nu_{i0}}n_{e0}$, this results in

$$I\overline{\nu_{i0}}n_{e0}=\int_{|\mathbf{w}|>\sqrt{2I/m}}K(w)\,\nu^{*}(w)n_{e0}\,\delta(\mathbf{w}-u\mathbf{e}_x)d\mathbf{w}$$
$$=K_u\nu^{*}(|u|)n_{e0}. \tag{15}$$

Then from Eqs. (14) and (15) we obtain

$$F_{\rm inel}/m=\overline{\nu_{i0}}uI/K_u. \tag{16}$$

In order to calculate the elastic part of the friction force we insert the elastic collision operator (7) into the integral on the right-hand side of the first of Eqs. (11), we use the distribution (12) for both functions $f(\mathbf{w})$ and $f(\mathbf{w}')$, and we perform triple integration over the variables $\mathbf{w}$, $\mathbf{w}_a$, and χ. Taking into account that (i) for the elastic collisions the Jakobian $\partial(\mathbf{w},\mathbf{w}_a)/\partial(\mathbf{w}',\mathbf{w}_a')$ equals one, (ii) for $\mathbf{w}'=u\mathbf{e}_x$ the x component of the vector $\mathbf{w}$ is $w_x=u\cos\chi$, and (iii) the changes of the atomic velocity due to elastic collisions with electrons can be neglected and, thus, $|\mathbf{w}-\mathbf{w}_a|=|\mathbf{w}'-\mathbf{w}_a'|$, we obtain the following expression for $F_{\rm el}/m$:

$$\frac{F_{\rm el}}{m}=\nu(|u|)u,$$

$$\nu(|u|)=N|u|\Sigma_{\rm el}(|u|),$$

$$\Sigma_{\rm el}(|u|)=2\pi\int_0^{\pi}\Sigma_d(|u|,\chi)(1-\cos\chi)\sin\chi\,d\chi. \tag{17}$$

Here $\Sigma_{\rm el}(|u|)$ represents the total elastic cross section with respect to momentum transfer for azimuthally symmetric elastic scattering [23].

The formula for the mean friction force on the tube axis, which takes into account the loss of the mean momentum due to ionizing the elastic collisions, may now be derived. For that purpose, the rate equation for electrons (1) at $r=0$ is presented in the form

$$\frac{\partial n_{e0}}{\partial t}+\mathrm{div}(n_e\mathbf{V})_{r=0}=(S)_{r=0}=\overline{\nu_{i0}}n_{e0}=\frac{F_{\rm inel}K_u n_{e0}}{muI}, \tag{18}$$

where the expression for the on-axis ionization source has been obtained with the aid of Eq. (16). Inserting Eq. (18) into the left-hand side of Eq. (5) allows us to calculate the mean acceleration on the axis

$$\frac{du}{dt}=\frac{\partial u}{\partial t}+u\frac{\partial u}{\partial x}=\frac{eE_0-F_{\rm eff}}{m},$$

$$\frac{F_{\rm eff}}{m}=\left(1+\frac{K_u}{I}\right)\frac{F_{\rm inel}}{m}+\frac{F_{\rm el}}{m}$$
$$=\mathrm{N}u^2[(1+I/K_u)\Sigma_i(K_u)+\Sigma_{\rm el}(K_u)], \tag{19}$$

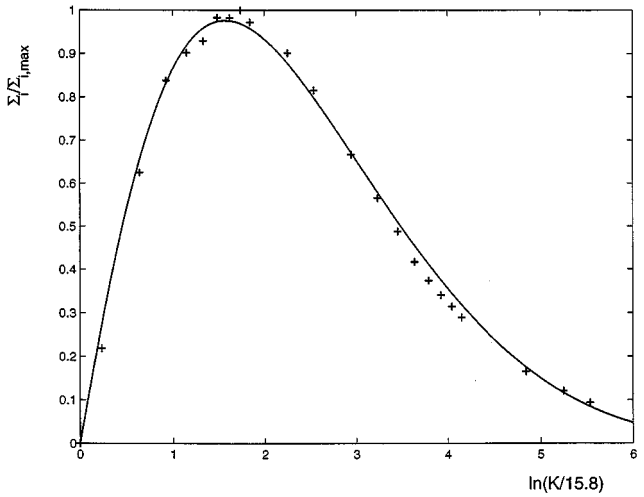

FIG. 2. Ionization cross section by electron-atom impact Σ_i for argon normalized by its maximal experimental value $(\Sigma_i)_{max} = 2.94 \times 10^{-16}\,cm^2$ as a function of the electron energy K given in eV and presented on a logarithmic scale. The signs (+) represent the experimental data of [21]. The solid curve is the analytical fit for Σ_i given by Eq. (68).

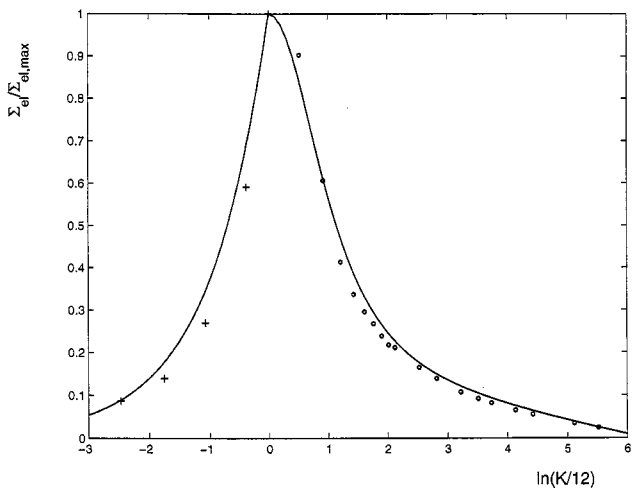

FIG. 3. Elastic electron scattering cross section for argon Σ_{el} normalized by its maximal experimental value $(\Sigma_{el})_{max} = 2.3 \times 10^{-15}\,cm^2$ as a function of the electron energy K given in eV and presented in the logarithmic scale. The circles and the signs (+) represent the experimental data of [21] and [26], respectively. The solid curve is the analytical fit for Σ_{el} given by Eq. (69).

where F_{eff} is the effective friction. As is seen from Eq. (19), the inelastic part of the effective friction force differs from the term F_{inel} related to the inelastic scattering of a single electron by a large factor $1 + K_u/I$. The additional term that is proportional to K_u/I appears due to the ionization process which increases the electron density and thus results in the lowering of the electron fluid velocity u that is the mean velocity calculated per one electron. When the direct ionization by electron-atom impact from the inner electronic shells is taken into account in calculating the effective friction, a single term associated with ionization is replaced by the sum of the terms $(1 + I_s/K_u)\Sigma_{is}(K_u)$. When investigating IWs, whose structure is characterized by the condition $I_s/K_u \ll 1$, the above-mentioned sum with an appropriate accuracy can be replaced by $(1 + I/K_u)\Sigma_{i,tot}$ where $\Sigma_{i,tot}(K_u)$ is the total ionization cross section which takes into account ionization from all shells.

Finally, the effective friction force F_{eff} used in our numerical simulations was determined by Eq. (19), in which Σ_i was replaced by $\Sigma_{i,tot}(K_u)$. For the total ionization cross section $\Sigma_{i,tot}(K)$ an analytical fit of experimental data for argon (see Fig. 2) given in [21] for $K < 4$ keV and in [25] for higher energies has been performed. An analytical fit was used also for the experimental cross section $\Sigma_{el}(K)$ of the elastic scattering of electrons by atoms of argon (Fig. 3). The experimental data for $\Sigma_{el}(K)$ presented in [21,22] and in [26] were employed in the range of energies $20\,eV < K < 6$ keV and for $K < 20$ eV, respectively.

In our numerical calculations the quantity K_u never exceeded 10 keV. No experimental data for $\Sigma_{el}(K)$ in argon were found in the literature for $K > 6$ keV. It was noticed that the Thomas-Fermi approximation [27], for which $\Sigma_{el}(K)$ decreases as $1/K^2$ for large K, is not applicable in the interval $6\,keV < K < 10\,keV$. For example, at $K = 6$ keV the Thomas-Fermi approximation results in the value of Σ_{el} which is much lower than the experimental value. This allowed the use of the simplest extrapolation of the curve shown in Fig. 3 assuming that $\Sigma_{el} = const$ for higher values of K up to 10 keV. Although such an extrapolation overestimates the actual values of $\Sigma_{el}(K)$ in the domain $6\,keV < K < 10\,keV$ and thus leads to the overestimation of the effective friction in that domain, it is appropriate when the parameters of the IW's are calculated numerically. Thus, it was checked that employing the power law $\Sigma_{el}(K) = \Sigma_{el}(K_0)(K_0/K)^2$ for $K > K_0 = 6$ keV practically did not change the numerical results. The reason is that for high electron energies the effective friction is much smaller than the electrostatic force. The same reason allowed us to neglect the loss of the electron momentum by the excitation of atomic levels. In the range of energies $K > 100$ eV the total excitation cross section for argon does not exceed 20% of the total ionization cross section [21], while the latter is about two times smaller than the total elastic cross section (compare Figs. 2 and 3). Therefore, the contribution of excitation to the effective friction force may be neglected in calculating the main characteristics of IWs in argon FCD.

III. QUASI-ONE-DIMENSIONAL MODEL OF PREBREAKDOWN STAGE OF FCD

In this section a closed system of equations is derived, for calculating the distributions of the electron and ion densities $[n_{e0}(x,t)$ and $n_{i0}(x,t)$, respectively], the electric field $E_0(x,t)$, and the electron velocity $u(x,t)$ on the capillary axis at the prebreakdown stage of a FCD. It is assumed that the characteristic length λ of the electric potential variation in the axial direction is much larger than the inner radius of the capillary a. Since the radial electric field and the radial electron velocity vanish at $r = 0$, the smallness of the ratio

$$a/\lambda = \alpha \ll 1 \tag{20}$$

results in small values of E_r/E_x and V_r/V_x inside the capillary. This allows the formulation of a quasi-one-dimensional

(Q1D) model for calculating the prebreakdown processes in a narrow capillary. The Q1D model should take into account the two-dimensional (2D) nature of the field and the electron flow as well as the electrodynamic boundary conditions at the capillary wall and at the conducting shield (see the similar approach for IWs in shielded discharge tubes in [11]). Clearly, the Q1D approach will result in more complicated equations in comparison with a strictly one-dimensional theory that ignores all radial effects. The advantage of the Q1D description is in the fact that it is based on a 1D system of partial differential equations (PDEs) instead of 2D PDEs.

We start with a full two-dimensional and time-dependent system of equations, which includes Eqs. (1) and (2) for the concentrations of electrons and ions, the Poisson equation for the electric potential $\varphi(x,r,t)$

$$\frac{\partial^2\varphi}{\partial x^2}+\frac{1}{r}\frac{\partial}{\partial r}\left(r\frac{\partial\varphi}{\partial r}\right)=\frac{e(n_i-n_e)}{\varepsilon_0}, \tag{21}$$

and the electron momentum equation for the electron velocity $\mathbf{V}(x,r,t)$

$$\frac{\partial\mathbf{V}}{\partial t}+(\mathbf{V}\cdot\boldsymbol{\nabla})\mathbf{V}=-\frac{(e\nabla\varphi+\mathbf{F}_{\rm eff})}{m}, \tag{22}$$

where $\mathbf{F}_{\rm eff}$ is given by vector generalization of the formula (19)

$$\mathbf{F}_{\rm eff}/m=P(V)\mathbf{V},$$

$$P(V)=N[(1+I/K_V)\Sigma_i(K_V)+\Sigma_{\rm el}(K_V)]V,$$

$$K_V=mV^2/2. \tag{23}$$

Unlike the electrostatic force, the friction force that is given by Eq. (23) is not a potential vector, i.e., $\boldsymbol{\nabla}\times\mathbf{F}_{\rm eff}\neq\mathbf{0}$, and it may generate vorticity $\boldsymbol{\omega}=\boldsymbol{\nabla}\times\mathbf{V}=\omega(x,r,t)\mathbf{e}_\theta$ in the electron fluid. However, the vortex part of the velocity field $\mathbf{V}$ is small in comparison with its potential part as is shown below.

A. Irrotational approximation for the electron velocity field

The equation for the distribution of vorticity ω satisfies an equation that can be obtained by applying the curl operator on both sides of the momentum equation (22). The result is

$$\frac{\partial\omega}{\partial t}+\mathbf{V}\cdot\boldsymbol{\nabla}\omega+\left(\frac{\partial V_x}{\partial x}+\frac{\partial V_r}{\partial r}+P(V)\right)\omega=\frac{dP}{dV}\left(V_x\frac{\partial V}{\partial r}-V_r\frac{\partial V}{\partial x}\right). \tag{24}$$

The right-hand side of Eq. (24) represents the source of vorticity, which vanishes identically in the case of a 1D flow. The total 2D velocity field can be expressed as a sum of potential and vortex parts by

$$\mathbf{V}=\mathbf{V}^{(p)}+\mathbf{V}^{(\omega)},\quad \mathbf{V}^{(p)}=\boldsymbol{\nabla}\Phi,\quad \mathbf{V}^{(\omega)}=\boldsymbol{\nabla}\times(\Psi\mathbf{e}_\theta), \tag{25}$$

where Φ is the velocity potential and Ψ is the stream function for the vortex component of the velocity field. The latter is determined by the equation

$$\nabla^2\Psi-\frac{\Psi}{r^2}\equiv\frac{\partial^2\Psi}{\partial x^2}+\frac{1}{r}\frac{\partial}{\partial r}\left(r\frac{\partial\Psi}{\partial r}\right)-\frac{\Psi}{r^2}=-\omega. \tag{26}$$

It is shown now that within the approximation employed in the current work, the vorticity may be neglected. As a first step toward that goal it is noticed that if $\omega=0$ at $t=0$ and if there is no vorticity influx to the capillary from the hollow cathode region, i.e., $\omega=0$ at $x=0$, then ω becomes nonzero for $x>0$ only due to the source on the right-hand side of Eq. (24). The vorticity generated in a narrow capillary can be presented as

$$\omega=A(x,t)r+O(r^2),\quad A(0,t)=0. \tag{27}$$

For the construction of a Q1D model a correct approximation for the radial velocity V_r is needed. Since in a shielded capillary the total radial velocity itself is small in comparison with the axial velocity, we have to check whether the vortex part of the radial velocity $V_r^{(\omega)}$ will be small in comparison with the potential part $V_r^{(p)}$. Expression (27) is inserted into Eq. (26) whose solution is then approximated as

$$\Psi=-A(x,t)r^3/8+O(r^4) \tag{28}$$

and, therefore,

$$V_r^{(\omega)}=-\partial\Psi/\partial x=(\partial A/\partial x)r^3/8+O(r^4). \tag{29}$$

To evaluate the function A and thus the magnitude of $V_r^{(\omega)}$ we consider the structure of the source term. The quantities $\partial V/\partial r$ and V_r vanish on the axis and for small values of r they behave linearly in r (as well as the radial electric field). Then, from Eq. (24) follows that $\omega=0$ on the axis and thus we may expect maximum vorticity near the wall. The derivative dP/dV is of the order of the inverse length of the electron momentum transfer $N\Sigma_m=1/\lambda_c$ [see Eq. (23)]. Therefore, for a narrow capillary filled with a low-density gas the source of vorticity is proportional to the small parameter

$$\alpha_c=a/\lambda_c\ll 1. \tag{30}$$

To estimate $V_r^{(\omega)}$ the source term in Eq. (24) is calculated to first approximation for the potential velocity field $\mathbf{V}=\mathbf{V}^{(p)}$. For a narrow capillary the 2D velocity potential Φ can be presented as

$$\Phi=\Phi_0(x,t)[1-\beta(x,t)r^2+O(r^3)]. \tag{31}$$

Here Φ_0 is the velocity potential on the axis and β is of order of $1/\lambda^2$, where λ is the characteristic axial length of both electric and velocity potentials variation. Then from the second of Eqs. (25) we obtain

$$V_x^{(p)}=\frac{\partial\Phi_0}{\partial x}-\frac{\partial(\beta\Phi_0)}{\partial x}r^2+O(r^3),$$

$$V_r^{(p)}=-2\beta\Phi_0 r+O(r^2), \tag{32}$$

and thus, the ratio $V_r^{(p)}/V_x^{(p)}$ is of the order of the parameter α defined in Eq. (20). Using approximation (32), the coefficients as well as the source term of Eq. (24) can be calculated. Inserting Eqs. (27) and (32) into Eq. (24) and collecting the terms linear in r lead to a first-order PDE (the transport equation) for the function $A(x,t)$

$$\frac{\partial A}{\partial t}+u(x,t)\frac{\partial A}{\partial x}+\Gamma(x,t)A=G(x,t), \tag{33}$$

where

$$u=\frac{\partial \Phi_0}{\partial x}, \quad \Gamma=\frac{\partial u}{\partial x}-2\beta\Phi_0+P(|u|),$$

$$G=2\left(\frac{dP}{dV}\right)_{V=|u|}\left[|u|\frac{\partial(\beta\Phi_0)}{\partial x}-\beta\Phi_0\frac{\partial|u|}{\partial x}+2\beta^2\Phi_0^2\,\mathrm{sgn}(u)\right]. \tag{34}$$

In principle, the solution $A(x,t)$ of Eq. (33) satisfying the conditions $A(x,0)=A(0,t)=0$ can be obtained by the method of characteristics (see, for instance, [28]). Applying that method would result in an expression for $A(x,t)$ in terms of integrals along the axial electron trajectories $x(t)$ given by $dx/dt=u(x,t)$. However, such a detailed calculation is not needed for evaluation of the order of magnitude of the solution $A(x,t)$. For transient processes associated with the propagation of IWs the second term on the left-hand side of Eq. (33) is of the order of the right-hand side term. Therefore, the order of magnitude of A is given by

$$|A|\approx\frac{\lambda|G|}{|u|}\approx\left|\frac{dP(u)}{du}\right|\beta\Phi_0\approx\frac{\beta\Phi_0}{\lambda_c}. \tag{35}$$

From Eqs. (29) and (35) we obtain

$$|V_r^{(\omega)}|\approx 0.1\frac{\beta\Phi_0 r^3}{\lambda\lambda_c}. \tag{36}$$

Finally, the ratio of the vortex radial velocity to its potential counterpart can be estimated now from Eq. (36) and the second of equations (32) as

$$\left|\frac{V_r^{(\omega)}}{V_r^{(p)}}\right|<\frac{0.1r^2}{\lambda\lambda_c}\leqslant 0.1\alpha\alpha_c\ll 1. \tag{37}$$

The vortex axial velocity $V_x^{(\omega)}$ vanishes on the axis ($r=0$). This is obtained from the equation $\mathrm{div}\,\mathbf{V}^{(\omega)}=0$ with the aid of Eq. (29). Therefore, in a narrow capillary $V_x^{(\omega)}$ is much less than its potential counterpart $V_x^{(p)}$. This result together with Eq. (37) means that the electron velocity can be described in the potential approximation. Neglecting the vorticity allows us to neglect the vortex part of the friction force and retain only its potential part, which is given by

$$\mathbf{F}_{\mathrm{eff}}^{(p)}/m=\nabla H. \tag{38}$$

Here mH is the force potential that can be found from the equation

$$\nabla^2 H\equiv\frac{\partial^2 H}{\partial x^2}+\frac{1}{r}\frac{\partial}{\partial r}\left(r\frac{\partial H}{\partial r}\right)=\vartheta,$$

$$\vartheta=\frac{\mathrm{div}\,\mathbf{F}_{\mathrm{eff}}}{m}=P\,\mathrm{div}\,\mathbf{V}+\frac{dP}{dV}\mathbf{V}\cdot\nabla V. \tag{39}$$

The source term in Eq. (39) can be calculated with the aid of Eqs. (23) and (32) and consequently the 2D solution for H can be obtained as a power series in r. Instead, a more simple 1D approximation for H is used below,

$$H=H(x,t)=\int_{x_0}^{x}P(|u(x',t)|)u(x',t)dx'. \tag{40}$$

The justification of this approximation is as follows. Since at the prebreakdown stage of the FCD the electrostatic force is much larger than the friction force, we may expect that the condition

$$\frac{|\mathbf{F}_{\mathrm{eff}}|}{|eE|}\approx\gamma=\frac{\lambda_E}{\lambda_c}\ll 1, \quad \lambda_E=\frac{K(u)}{|eE|}, \quad \lambda_c=\frac{1}{N\Sigma_m} \tag{41}$$

is satisfied at the leading edge of an IW. Here λ_E is the characteristic length of the collisionless electron acceleration, on which the kinetic energy acquired by the electron is of the order of the electric potential drop, and λ_c is the characteristic mean free path length of the electron. Numerical simulations presented in Sec. IV show that at the leading edge of an IW the parameter γ is of the order of 0.1 or less. A small γ does not mean that the friction force can be neglected since it is strongly coupled with the ionization effect. Clearly, in the Q1D approximation the friction force should be taken into account in the axial projection of the momentum equation. At the same time, due to the condition $V_r/V_x\ll 1$ that follows from Eq. (20) the radial component of the friction force may be neglected. Taking the latter into account would result in a higher order ($\alpha\alpha_c\ll\alpha$) correction to the radial velocity. At the trailing edge of an IW the friction and the electrostatic force are in equilibrium and the parameter γ becomes of order one. In spite of this, the radial component of the friction force can be neglected also at the trailing edge since behind the IW both radial field and radial velocity practically vanish due to high plasma conductivity. Thus, the force potential H is given by Eq. (40) that represents the solution of Eq. (39), in which the source term is replaced by its value on the axis $\vartheta(x,r=0,t)$.

For the electron momentum equation (22) presented in the form

$$\frac{\partial\mathbf{V}}{\partial t}+(\mathbf{V}\cdot\nabla)\mathbf{V}=-\nabla\left(\frac{e\varphi}{m}+H\right). \tag{42}$$

with $\mathbf{V}=\nabla\Phi$, the following integral that couples of all three potentials Φ, φ, and H may be obtained:

$$\frac{\partial\Phi}{\partial t}+\frac{(\nabla\Phi)^2}{2}+\frac{e\varphi}{m}+H=g(t), \tag{43}$$

where $g(t)$ is an arbitrary function of time. Since an arbitrary function of time can be added to the velocity potential Φ without any changes in the velocity field, we may assume $g(t)=0$. The relationship (43) is of the same type as the Cauchy-Lagrange integral that appears in the theory of time-dependent irrotational flows in the presence of potential forces (see, for instance, [29]). Equation (43) will be used below for calculating the function $\beta(x,t)$ and coupling the radial velocity with on-axis distributions.

B. Waveguide approach for the electric potential

Consider now the structure of the 2D electric potential and the electrodynamic boundary conditions. For a narrow capillary the electric potential can be presented as

$$\varphi(x,r,t)=\varphi_0(x,t)J_0[k(x,t)r]$$
$$=\varphi_0(x,t)[1-k^2(x,t)r^2/4+O(r^3)]$$
$$(0\leqslant r\leqslant a,\quad k^2a^2\ll 1). \quad (44)$$

Here J_0 is the Bessel function of zero order, $k(x,t)$ is an unknown function which will be determined from the boundary conditions at the plasma-dielectric interface ($r=a$) and at the conducting shield ($r=R$). In the plasma domain the electric field $\mathbf{E}=-\nabla\varphi$ is calculated from Eq. (44)

$$E_x=-\frac{\partial\varphi_0}{\partial x}J_0(kr)=-\frac{\partial\varphi_0}{\partial x}+O(r^2),$$

$$E_r=\varphi_0 kJ_1(kr)=\frac{k^2\varphi_0 r}{2}+O(r^2)\quad (0\leqslant r<a). \quad (45)$$

In the dielectric spacer the electric potential distribution satisfies the Laplace equation with boundary conditions $\varphi(x,a+0,t)=\varphi(x,a-0,t)$ and $\varphi(x,R,t)=0$. As a result, the following approximation is employed:

$$\varphi(x,r,t)=\varphi_0(x,t)J_0(ka)\frac{N_0(kR)J_0(kr)-J_0(kR)N_0(kr)}{N_0(kR)J_0(ka)-J_0(kR)N_0(ka)}$$
$$(a\leqslant r\leqslant R), \quad (46)$$

where N_0 is the Neumann function of zero order. Notice that k is still unspecified. It will be later determined by the continuity of the total normal current density at $r=a$.

The radial profiles for the electric potential in the forms (44) and (46) are chosen by the same reasons as in the theory of ionization waves in long shielded discharge tubes filled with a weakly ionized plasma [see Chap. 4 in [11] for details]. The leading edge of an IW actually represents a linear potential wave propagating in a shielded tube as in a plasma waveguide, for which the electric field decays in space exponentially towards the cathode. The presence of the conducting shield $r=R$ having the cathode potential is the cause of the field decay from the anode to the cathode. In the limit of an infinitely long tube when the cathode position is at $x=-\infty$, the linear potential wave propagating in the negative x direction is described by Eqs. (44) and (46) with a constant waveguide parameter $k=\tilde{k}$ and with $\varphi_0\propto\exp[k(x+Wt)]$, where $W>0$ is the wave velocity. Therefore, the parameter k represents also the inverse characteristic length of the electric field decay at the leading edge of an IW. The linear potential waves are exact solutions of the Laplace equation for both plasma and dielectric domains. Expressions (44) and (46) satisfy the condition for continuity of the electric potential at the plasma-dielectric interface as well as at the conducting shield. The second boundary condition that should be satisfied at the plasma-dielectric interface has the form

$$(j_r+\varepsilon_0\partial E_r/\partial t)_{r=a-0}=\varepsilon\varepsilon_0(\partial E_r/\partial t)_{r=a+0}. \quad (47)$$

Here j_r is the radial component of the conduction current density. Equation (47) represents the condition for continuity of the total radial current density at $r=a$, including the displacement radial current in both domains. It describes the process of charging the distributed capacitor formed by the plasma-dielectric interface and the conducting shield. In the linear theory the quantity j_r is related to E_r as

$$j_r=en_eE_r/[m(kW+\nu)]. \quad (48)$$

Here ν is the mean frequency of the elastic electron-atom collisions in the nonperturbed plasma. It is assumed that far ahead of the ionization front the mean energy of the electrons is low and the inelastic collisions can be neglected. The dispersion relation [30] that guarantees the existence of nontrivial solutions in the form of exponential waves $\propto\exp[k(x+Wt)]$ may be derived from Eqs. (44)–(48),

$$\Lambda(ka,R/a)\equiv\frac{J_0(ka)[J_1(ka)N_0(kR)-J_0(kR)N_1(ka)]}{J_1(ka)[J_0(ka)N_0(kR)-J_0(kR)N_0(ka)]}$$
$$=\Theta(kW),$$

$$\Theta(kW)=\frac{kW(kW+\nu)+\omega_p^2}{\varepsilon kW(kW+\nu)},\quad \omega_p^2=\frac{e^2n_e}{m\varepsilon_0}. \quad (49)$$

Here ω_p is the plasma frequency ahead of the ionization front; J_1 and N_1 are the Bessel and Neumann functions of first order, respectively. For a given wave velocity W relation (49) is a transcendental equation for k. This equation has an infinite number of roots corresponding to all possible waves (the eigenmodes) that may propagate in a plasma waveguide in the absence of applied external field. The eigenmode, which describes the leading edge of an IW, has the lowest radial nonuniformity of the electric potential in the plasma domain and it is determined by the minimal positive root of Eq. (49). To construct a Q1D model of IWs in an inhomogeneous plasma we assume that in each cross section of the capillary ($x=$const) the radial profile of the electric potential is similar to the profile prescribed by the linear theory. However, now the on-axis potential $\varphi_0(x,t)$ is not presented by some exponential function and the waveguide parameter k is not a constant as in the case of linear waves. Inserting Eq. (44) into the Poisson equation (21) and collecting the terms that are independent of the radial coordinate r results in a differential equation for the on-axis potential

$$\frac{\partial^2\varphi_0}{\partial x^2}-k^2(x,t)\varphi_0=\frac{e(n_{i0}-n_{e0})}{\varepsilon_0}, \quad (50)$$

which contains an unknown waveguide parameter $k(x,t)$. Both functions $\varphi_0(x,t)$ and $k(x,t)$ should be calculated self-consistently from the Q1D theory that takes into account ionization and all relevant nonlinear phenomena. Inserting Eqs. (44)–(46) into Eq. (47) results in a differential equation that can be considered as a generalization of the dispersion relation (49) to the case of nonexponential wave solutions

$$\frac{\partial[kJ_1(ka)[\varepsilon\Lambda(ka,R/a)-1]]}{\partial k}\frac{\partial k}{\partial t}+kJ_1(ka)$$

$$\times[1-\varepsilon\Lambda(ka,R/a)]\frac{\partial \ln\varphi_0}{\partial t}+\frac{j_{rw}}{\varepsilon_0\varphi_0}=0. \quad (51)$$

Here j_{rw} is the radial component of the conduction current in the plasma at $r=a$ determined by

$$j_{rw}=-2en_w\beta a\Phi_0, \quad (52)$$

where $n_w(x,t)$ is the concentration of electrons on the inner wall of the capillary and $\beta(x,t)$ is the parameter in expansion (31) for the velocity potential. The parameter β appears in the Q1D model not only in Eq. (51) for the waveguide parameter k but also in Eq. (18) for the on-axis concentration of electrons since the latter contains the value of div$\mathbf{V}$ on the axis. Inserting this quantity calculated from Eq. (32) into Eq. (18) results in

$$\frac{\partial n_{e0}}{\partial t}+u\frac{\partial n_{e0}}{\partial x}+\left(\frac{\partial u}{\partial x}-4\beta\Phi_0\right)n_{e0}=\frac{F_{\text{inel}}K_u n_{e0}}{muI}. \quad (53)$$

The equation for the on-axis concentration of ions is given by

$$\frac{\partial n_{i0}}{\partial t}=\frac{F_{\text{inel}}K_u n_{e0}}{muI}. \quad (54)$$

In the particular case of linear potential waves, for which

$$k=\tilde{k}=\text{const}, \quad \frac{\partial \ln\varphi_0}{\partial t}=\tilde{k}W=\text{const}, \quad \beta=\frac{\tilde{k}^2}{4},$$

$$j_{rw}=\frac{e^2\tilde{n}_w(E_r)_{r=a-0}}{m(\tilde{k}W+\nu)}, \quad (E_r)_{r=a-0}=\tilde{k}J_1(\tilde{k}a)\varphi_0,$$

$$\tilde{n}_w=\text{const}, \quad (55)$$

Eq. (51) is reduced to Eq. (49). Here $\tilde{n}_w$ is the electron density on the inner wall of the capillary $r=a-0$.

Equation (49) is used for the formulation of the asymptotic conditions at the leading edge of the IW. It allows calculating the wave velocity W in terms of the asymptotic value of the waveguide parameter $\tilde{k}$ and the parameters of weakly ionized plasma at the leading edge of the IW. The latter are determined by the characteristics of the electron beam at the cathode end of the capillary. Replacing k in Eq. (49) by $\tilde{k}$ and multiplying that equation by $(\tilde{k}W+\nu)W$ results in a quadratic equation for W, whose positive solution is given by

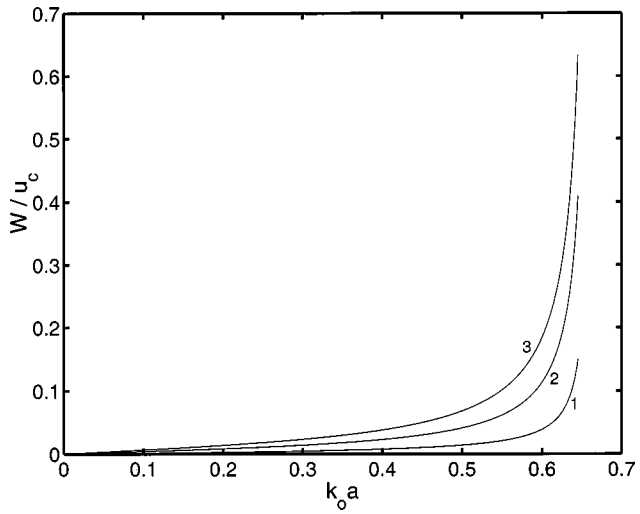

FIG. 4. The wave velocity W normalized by $u_c=\sqrt{2I/m}=2.36\times10^8$ cm/s as a function of the parameter k_0a for a cylindrical plasma waveguide with $\varepsilon=5$, $R/a=4$, $b/a=0.63$ filled with an argon plasma at pressure $p=600$ mTorr. Curves 1, 2, and 3 correspond to initial concentrations of electrons $n_{e0}=10^{10}\,\text{cm}^{-3}$, $3\times10^{10}\,\text{cm}^{-3}$ and $5\times10^{10}\,\text{cm}^{-3}$, respectively.

$$W=-\frac{\nu}{2\tilde{k}}+\sqrt{\frac{\nu^2}{4\tilde{k}^2}+\frac{\tilde{\omega}_p^2}{\tilde{k}^2[\varepsilon\Lambda(\tilde{k}a,R/a)-1]}}, \quad \tilde{\omega}_p^2=\frac{e^2\tilde{n}_w}{m\varepsilon_0}. \quad (56)$$

Equation (56) is used only if $\tilde{k}$ belongs to the interval $0<\tilde{k}<k_m$ which corresponds to the first (large-scale) waveguide eigenmode. Only such large-scale eigensolutions are relevant for the modeling of IWs within the framework of the Q1D approach. The quantity k_m that is the upper permitted value of $\tilde{k}$ depends on the dielectric permittivity of the tube's wall ε and on both geometric parameters a and R. This limiting value is defined as the minimal positive root of the equation

$$\varepsilon\Lambda(k_ma,R/a)-1=0. \quad (57)$$

The quantity k_ma, which depends on two parameters, ε and R/a, increases with ε and decreases with R/a. In the interval $0<\tilde{k}<k_m$ the wave velocity W increases monotonically with the wave number $\tilde{k}$. The wave velocity increases also with the increase of the electron density $\tilde{n}_w$. Typical behavior of $W(\tilde{k})$ calculated numerically from Eq. (56) for various values of $\tilde{n}_w$ is shown in Fig. 4, where k_0 is identified with $\tilde{k}$. It should be noted that Eq. (56) predicts an infinite wave velocity for $\tilde{k}=k_m$. This result is a consequence of the potential approximation for the electric field ($\mathbf{E}=-\nabla\varphi$) used in the present model. This approximation fails when the wave velocity approaches the velocity of electromagnetic wave propagation in a dielectric medium and, therefore, in that range of velocities the dispersion relation (49) should be modified. The potential approximation is valid if $\varepsilon W^2/c^2\ll1$, where c is the vacuum speed of light. Actually this condition is satisfied for all values of W obtained in numerical simulations of IWs. For a given value of $\tilde{k}a$, the wave velocity W increases with the increase of the ratio R/a of the shield radius to the inner

capillary radius. For a given geometry and for a fixed value of $\tilde{n}_w$ the quantity W decreases with the increase of the frequency of elastic collisions ν, i.e., with the increase of the initial density N_0 of the gas. However, it does not mean that the velocity of an IW is expected to be a decreasing function of N_0 since for low initial gas densities the electron density of a beam injected to the capillary from the HCR does not remain constant but increases with the increase of N_0. Analysis of Eq. (56) shows that a linear or more rapid increase of $\tilde{n}_w$ with N_0 provides an increasing dependence of the wave velocity on N_0, i.e., on the initial pressure of the gas in the HCR. Actually for a given pressure of the gas and for a given applied voltage the wave velocity can be calculated only from the solution of the full nonlinear problem. Although the quantity W can be calculated from Eq. (56), the asymptotic value of the waveguide parameter $\tilde{k}$ entering into this formula *is not given a priori* and it is determined by the maximal value of the on-axis potential obtained in the nonlinear solution (see Sec. IV, in which the solutions for IWs are presented).

In the present model the ratio of the on-wall electron concentration n_w to the on-axis concentration n_{e0} should be given as an additional parameter. It can be related to the effective electron beam radius b if a Gaussian distribution of the electron density in the radial direction is assumed

$$n_e(x,r,t)=n_{e0}(x,t)\exp(-r^2/b^2),$$

$$n_w/n_{e0}=\exp(-a^2/b^2). \tag{58}$$

The quantity b can be taken from experiment or from calculations performed for the HCR. To complete the system of Q1D equations, an equation for the parameter β should be obtained. This can be done by inserting Eqs. (31) and (44) into Eq. (43). Collecting the terms of Eq. (43) that are independent of r results in an equation for the on-axis velocity potential Φ_0, whose derivative with respect to x leads to Eq. (19) for the on-axis velocity u. Collecting the terms of Eq. (43) that are proportional to r^2 leads to the needed equation for β

$$\left(1-\frac{mu^2}{2e\varphi_0}\right)\beta-\frac{k^2}{4}=\frac{m\Phi_0}{e\varphi_0}\left(\frac{\partial\beta}{\partial t}+u\frac{\partial\beta}{\partial x}-\frac{H\beta}{m\Phi_0}-2\beta^2\Phi_0\right). \tag{59}$$

The parameters of the expected solutions that describe the IWs satisfy the conditions

$$\lambda_u/\lambda_\beta\ll 1, \quad |\beta|\lambda_u^2\ll 1, \tag{60}$$

where λ_u is the characteristic length of the electron acceleration and λ_β is the characteristic length of variation of the parameter β. Conditions (60) mean that the right-hand side of Eq. (59) is small and, therefore, a local approach relating β to the waveguide parameter k can be used

$$\beta=\frac{k^2}{4(1+K_u/|e|\varphi_0)}, \quad K_u=\frac{mu^2}{2}. \tag{61}$$

Thus, a closed system of Q1D equations has been derived. This system contains three 1D first-order partial differential equations (19), (53), and (54) for the on-axis distributions of the electron velocity, electron and ion concentrations, respectively, a second-order ordinary differential equation (50) for the on-axis electric potential, and a first-order ordinary differential equation (51) for the parameter k. An additional ordinary differential equation is needed for calculating the on-axis velocity potential Φ_0

$$\partial\Phi_0/\partial x=u. \tag{62}$$

The function Φ_0 appears in Eq. (53) for the electron density and in Eq. (51) for the parameter k through the radial current density on the wall that is given by Eq. (52). The on-axis electric field that is needed for the solution of the electron momentum equation (19) is determined by

$$E_0=-\partial\varphi_0/\partial x. \tag{63}$$

The ionization source in Eqs. (53) and (54) is calculated with the aid of Eqs. (16) and (13). The effective friction force in the electron momentum equation is given by the second of Eqs. (19). The function $\beta(x,t)$ is calculated from Eq. (61). Other parameters, such as the capillary radius a, the shield radius R, the beam radius b, the dielectric permittivity ε of the capillary wall, and the concentration of atoms N should be specified as well as the initial and boundary conditions.

The system of QID equations obtained in the present section allows calculating various transient processes related to electron fluid dynamics in a self-consistent electric field and to ionization growth in a FCD. If such parameters as the initial particle density of the background gas N_0, the capillary radius a, the effective beam radius b, the shield radius R, and the dielectric permittivity ε are constant, the coefficients of QID equations do not depend explicitly on the coordinate x. In this case the QID equations admit self-similar solutions in the form of traveling waves that are described in the next section.

IV. NUMERICAL SIMULATION OF STATIONARY IONIZATION WAVES

In the present section the self-similar solutions of a system of QID equations are considered. Such solutions depend only on one variable

$$\xi=x+Wt, \tag{64}$$

where $W>0$ is a constant wave velocity. The self-similar solutions represent steady-state waves, whose form does not change in the process of wave propagation. Solutions are sought that describe a simultaneous propagation of the virtual anode and the ionization front in a FCD from the anode to the cathode hole. Although mathematically self-similar solutions are defined in the whole range $-\infty<\xi<\infty$, they may describe IWs propagating in a capillary with a finite length if the latter is much larger than the characteristic thickness of the ionization front. To calculate self-similar solutions we have to solve a system of ordinary differential equations (ODEs) that is obtained from a QID system of PDEs if in the latter the partial derivatives with respect to coordinate x and time t are replaced by

$$\partial/\partial x=d/d\xi, \quad \partial/\partial t=Wd/d\xi. \tag{65}$$

Employing relations (65) in the QID equations results in a seventh-order system of ODEs for seven unknown functions of the variable ξ—the on-axis electric field E_0 and the electric potential φ_0, the on-axis velocity of electrons u and its potential Φ_0, the on-axis concentrations of ions n_{i0} and electrons n_{e0}, and the waveguide parameter k. Since only on-axis distributions will be considered in this section, the subscript ''zero'' referred to these distributions will be omitted henceforth. Defining the vector solution $\mathbf{y}(\xi)$, whose components are the seven unknown functions

$$\mathbf{y}(\xi)=(E,\varphi,u,\Phi,n_i,n_e,k) \tag{66}$$

and the constant vector $\mathbf{h}$ containing the parameters N_0, a, b, R, and ε, we present the system of ODEs in the form

$$\frac{d\mathbf{y}}{d\xi}=\mathbf{q}(\mathbf{y};\mathbf{h},W), \tag{67}$$

where $\mathbf{q}$ is a known vector function. The components of the vector $\mathbf{q}$ are derived from the QID equations and described by quite cumbersome formulas, which are not presented here.

As an example, the properties of IWs in argon were investigated. The ionization cross section Σ_i and the elastic cross section Σ_{el} as functions of electron energy were fitted analytically to experimental data for argon as

$$\Sigma_i=3.545\times10^{-16}\frac{\ln z+0.97\ln^2 z}{z+0.003\,906z^2}\,\mathrm{cm}^2$$

$$(1\leqslant z<500,\quad z=K_u/15.8) \tag{68}$$

and

$$\Sigma_{\mathrm{el}}=2.29\times10^{-15}B(\zeta)\,\mathrm{cm}^2\quad[\zeta=\ln(K_u/12)],$$

$$B(\zeta)=\begin{cases}1+0.9955(e^{\zeta}-1) & (\zeta<0)\\ 1-0.6333\zeta^2/(1-0.3065\zeta+0.7842\zeta^2-0.02024\zeta^3)\end{cases}$$

$$(0<\zeta<6.3). \tag{69}$$

In Eqs. (68) and (69), K_u is the electron energy in eV. The experimental curves as well as their analytical fits are shown in Figs. 2 and 3.

The system of ODEs (67) was integrated numerically in the interval $0<\xi<L=15\,\mathrm{mm}$ for $a=0.4\,\mathrm{mm}$, $b=0.19\,\mathrm{mm}$, $R=1.6\,\mathrm{mm}$, $\varepsilon=5$, and various initial pressures of argon in the range of 450–900 mTorr. The initial conditions for the system (67) were specified for all components of the vector $\mathbf{y}$ at $\xi=0$

$$\mathbf{y}(\xi=0)=\mathbf{y}_0. \tag{70}$$

The initial conditions (70) specify the values of the electric field as well as the parameters of the weakly ionized plasma at the cathode end of the capillary, i.e., ahead of the ionization front when the virtual anode begins to propagate. Such initial conditions are formulated with the aid of the linear theory of electric potential waves propagating in a plasma waveguide. The linear potential wave, for which the electric potential behaves as $\exp(k\xi)$, describes the leading edge of the ionizing nonlinear potential wave propagating with the same velocity W. To switch-on the ionization process in the beginning of the numerical calculation, it was assumed that both the kinetic energy of the incoming electrons and the electric potential are equal to the ionization potential $I=15.8\,\mathrm{eV}$. This value is very small in comparison with the electric potential of the virtual anode, which is of order of 10 keV, so that the linear theory is applicable and, thus, the electric field is related to the electric potential at $\xi=0$ as

$$E_0=-k_0\varphi_0. \tag{71}$$

The initial electron and ion concentrations $n_{e0}\approx n_{i0}$ were chosen in the range 10^{10}–$10^{11}\,\mathrm{cm}^{-3}$, which is expected for the initial beam electrons ejected to the capillary from the cathode hole. It was assumed that the initial electron density increases linearly with the initial gas pressure ($n_{e0}/N_0=\mathrm{const}$). In the numerical calculations the initial waveguide parameter k_0 was varied in the vicinity of the maximum permitted value k_m calculated from Eq. (57). For each selected value of k_0 the wave velocity W was calculated from Eq. (56) with $\tilde{k}=k_0$ and that value of W was used in the numerical integration. Both parameters k_0 and W were determined by the nonlinear solution describing IW, for which a given maximum value of the electric potential φ_m was achieved. Thus, the calculated wave velocity was determined as a function of the gas pressure and the maximal potential φ_m.

To avoid calculations of the Bessel and Neumann functions at each step of the integration and to reduce computing time, the function $D=kaJ_1(ka)[\varepsilon\Lambda(ka,R/a)-1]$ that appears in Eq. (51) was calculated for given values of a, R, and ε as a function of k. For $\varepsilon=5$, $R/a=4$ it was found that $D(ka)$ in the interval $0<(ka)^2<(k_ma)^2=0.436$ is well approximated by a simple rational function

$$D\approx\tilde{D}(ka)=\frac{4.16[(k_ma)^2-(ka)^2}{1-0.279(ka)^2} \tag{72}$$

and this function was used for integrating Eq. (51).

Typical distributions of the physical parameters as functions of the variable $\xi=x+\mathrm{Wt}$ obtained in the numerical simulations of the steady-state IWs are shown in Figs. 5–12. As mentioned before, all distributions are on axis. The IW propagates from right to left: The points $\xi=0$ and $\xi=L=15\,\mathrm{mm}$ correspond to the leading and trailing edges of the IW, respectively. The distributions shown in Figs. 5–12 are calculated for the wave velocity $W=2\times10^8\,\mathrm{cm/s}$ which corresponds to the virtual anode potential, i.e., the maximum value of the on-axis electric potential $\varphi(\xi)$ within the IW structure, $\varphi_m\approx12\,\mathrm{kV}$ for the initial gas pressure $p=600\,\mathrm{mTorr}$ ($N_0=2\times10^{16}\,\mathrm{cm}^{-3}$) and for the initial concentration of electrons ahead of the IW front $n_{e0}=6\times10^{10}\,\mathrm{cm}^{-3}$.

The peak of the distribution of $\varphi(\xi)$ which is seen in Fig. 5 is created due to the reversal of the direction of the axial electric field $E(\xi)$. The distribution $E(\xi)$ is shown in Fig. 6, where the reversal of the electric field and the train of high-frequency oscillations ended by a low constant residual field are seen. The on-axis distribution of the space charge is pre-

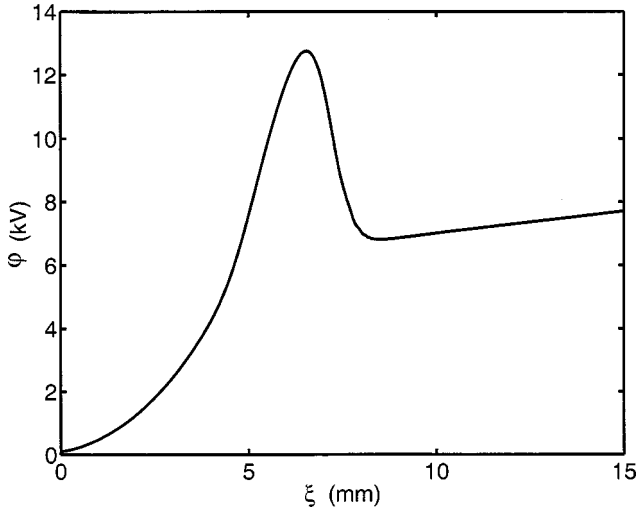

FIG. 5. The on-axis electric potential φ as a function of the variable $\xi = x + Wt$ for a cathode-directed IW propagating in a shielded capillary with $a = 0.4$ mm, $b = 0.19$ mm, $R = 1.6$ mm, $\varepsilon = 5$ filled with argon at pressure $p = 600$ mTorr, and $n_{e0} = 6 \times 10^{10}$ cm^{-3}. The virtual anode peak propagates to the left with the velocity $W = 2 \times 10^8$ cm/s.

sented in Fig. 7, which shows a long positively charged domain adjoining to the leading edge of the IW and a well-defined wave packet of high-frequency oscillations with a solitary envelope. The distribution of the on-axis electron velocity $u(x)$ is shown in Fig. 8, which demonstrates the stages of the electron acceleration at the leading edge and deceleration within the structure of IW. The deceleration is mainly due to the sign reversal of the electric field.

Figure 9 demonstrates the distribution of ion density $n_i(\xi)$ which has a steplike shape. Figures 9 and 5 together demonstrate that the obtained solution indeed represents an IW that is accompanied by virtual anode propagation. Figure 10 shows the distribution of the parameter $\eta(\xi) = 1 - n_e(\xi)/n_i(\xi)$, which characterizes the deviation of the electron-ion gas from quasineutrality. As is clearly seen from

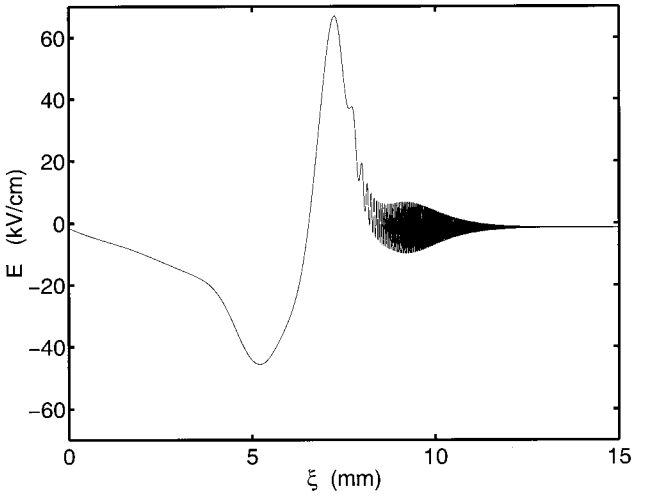

FIG. 6. The on-axis distribution of the axial electric field $E(\xi)$. The distributions shown in this figure and in Figs. 7–12 have been calculated for the same IW, whose parameters are indicated in the caption to Fig. 5.

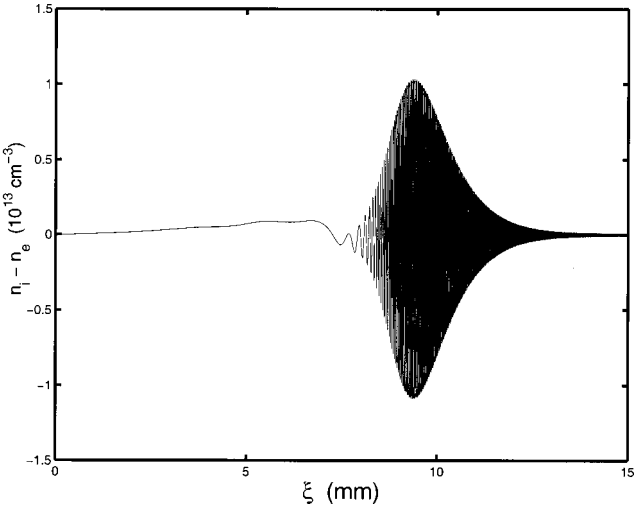

FIG. 7. The on-axis distribution of $n_i(\xi) - n_e(\xi)$ demonstrating the behavior of the space charge within the IW structure.

this figure, a strong violation of quasineutrality takes place at the leading edge of the IW, while the electron-ion gas at the trailing edge represents a regular plasma system characterized by the condition $|\eta| \ll 1$. Figure 11 shows the distribution of the total axial electric current $J(\xi)$, which includes both conduction and displacement components. The current increases at the leading edge, undergoes high-frequency oscillations within the IW structure, and finally reaches a constant value at the trailing edge where the displacement current is very small. The behavior of the waveguide parameter $k(\xi)$ is shown in Fig. 12. This parameter decreases monotonically and vanishes at the trailing edge of the IW. Such a behavior of $k(\xi)$ indicates that the two-dimensional nature of the electric field at the leading edge of IW changes and becomes purely axial and one dimensional at the trailing edge.

The main features of the IW structure do not change within the investigated range of the initial gas pressure p. The increase of p results in the increase of the wave velocity W and in the lowering of the maximum velocity of the accelerated electrons u_m. The ion density behind the ionization

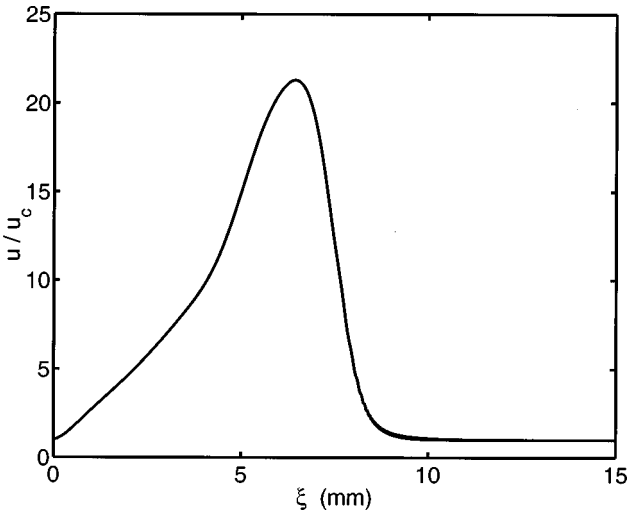

FIG. 8. The on-axis distribution of the electron velocity $u(\xi)$ normalized by u_c for the IW.

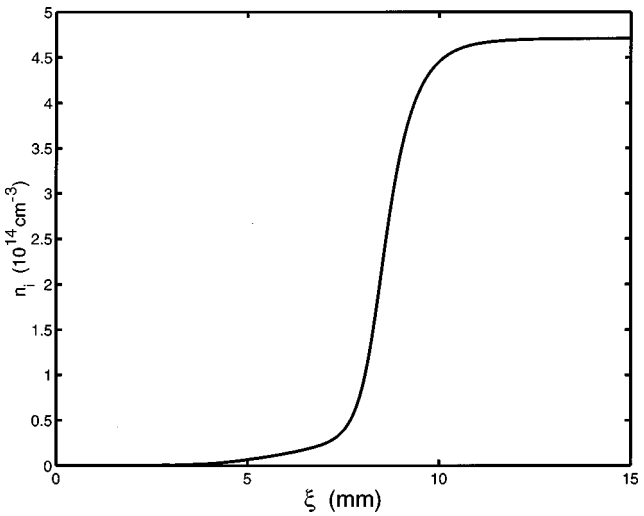

FIG. 9. The on-axis distribution of the ion density $n_i(\xi)$ for the IW.

front $n_i(L)$ and the electric current at the trailing edge of the IW, $J(L)$, increase with the increase of the gas pressure. The plasma behind the IW is not yet fully ionized. The ionization degree at the trailing edge $n_i(L)/N_0$ is close to 0.02 and it slightly increases with pressure in the range $p = 450-900$ mTorr. The characteristic values of the main physical parameters of the IWs calculated for various values of p are given in Table I.

For a given value of the gas pressure, the wave velocity increases very weakly with the increase of the virtual anode potential φ_m. It was found that in the range $\varphi_m = 10-20$ kV the wave velocity practically does not depend on φ_m.

V. DISCUSSION AND CONCLUSIONS

The theoretical approach developed in the present paper is intended for the modeling of cathode-directed IWs propagating in shielded capillaries. The model is applicable to the range of relatively high values of E/N, for which the characteristic time of the electron acceleration in the electric field is much shorter than the characteristic time of the electron-neutral particle collisions. This allows calculating both the ionization source and the dynamic friction in the beamlike approximation for the electron distribution function. In addition, it is assumed in the present model that not only the capillary aspect ratio is large ($L/a \gg 1$) but also the ratio of the characteristic length of the axial variation of the electric potential to the capillary radius is a large parameter. This allows the formulation of a quasi-one-dimensional model for calculating IWs in a fast capillary discharge. Within the framework of the validity of the model, typical parameters of IWs can be seen from the results of numerical calculations performed for argon and presented in Sec. IV.

The theoretical study of IWs presented in this paper shows that the qualitative properties of IWs propagating in an electron-beam-assisted FCD are quite different from the properties of IWs investigated for other kinds of pulse discharge. Although some common features of IWs in FCD and

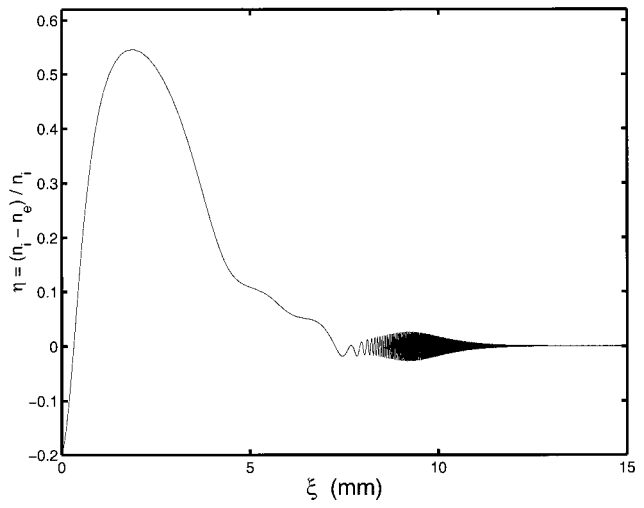

FIG. 10. The distribution of $\eta(\xi) = 1 - n_e(\xi)/n_i(\xi)$ describing the deviation from quasineutrality within the IW structure.

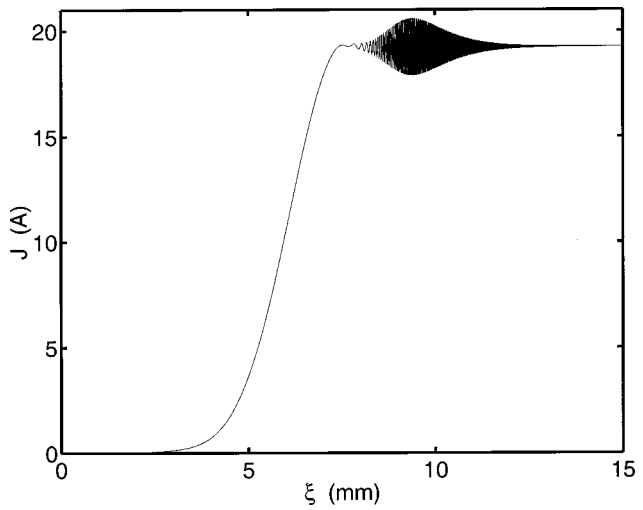

FIG. 11. The total axial electric current $J(\xi)$ transferred by the IW. The function $J(\xi)$ represents the integral of the sum $en_eV_x + \varepsilon_0 \partial E_x/\partial t$ over the capillary cross section $0 < r < a$.

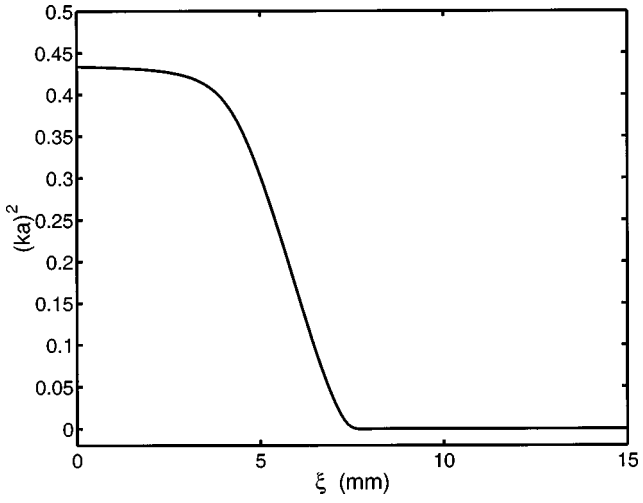

FIG. 12. The distribution of the quantity $(ka)^2$ within the IW structure. The waveguide parameter $k(\xi)$ is calculated from Eq. (51).

TABLE I. Characteristic parameters of IWs for a given virtual anode potential $\varphi_m = 12$ kV and for various gas pressures p. Here W is the wave velocity, $u_{\max}$ is the maximum value of the on-axis electron velocity, $n_i(L)$ is the ion density at the anode end of the capillary ($\xi = L$) behind the ionization front, $n_i(L)/N_0$ is the ionization degree achieved behind the IW, $J(L)$ is the total axial electric current behind the IW, $|E_1|$ is the magnitude of the first peak of the electric field within the IW structure.

p (mTorr)	450	600	900
W (cm/s)	1.4×10^8	2.0×10^8	3.1×10^8
$u_{\max}$ (cm/s)	5.2×10^9	4.9×10^9	4.1×10^9
$n_i(L)$ (cm^{-3})	3.1×10^{14}	4.6×10^{14}	7.6×10^{14}
$n_i(L)/N_0$	0.021	0.023	0.025
$\max\lvert n_i-n_e\rvert$ (cm^{-3})	2.7×10^{13}	1.1×10^{13}	2.2×10^{12}
$J(L)$ (A)	12	19	31
$\lvert E_1\rvert$ (kV/cm)	45	47	43

in preionized shielded discharge tubes described in [11] are revealed, such as the two-dimensional nature of the electric field at the leading edge of the IW, some distinct features of IWs in FCD are evident. The first of them is the strong acceleration of the near-axis electrons in the electric field at the leading edge of the IW followed by a strong deceleration in the reversed field (see Fig. 8). The wave velocity is much less (about 20 times) than the peak value of the mean electron velocity. Such conditions never were achieved in conventional fast IWs propagating in discharge tubes at lower values of E/N. The role of the inertial term which was retained in the electron momentum equation is very important for the formation of the electron velocity distribution $u(\xi)$ shown in Fig. 8. Unlike the electric field distribution $E(\xi)$, which after the first sign reversal oscillates with the increasing plasma frequency and changes direction many times before a small constant cathode-directed field is established at the trailing edge of the IW (see Fig. 6), the amplitude of the electron velocity oscillation is very small. This small oscillation is superimposed on a slowly varying average electron velocity that exceeds the critical velocity $u_c = \sqrt{2I/m}$ corresponding to the ionization switch on. As a result, the direction of the electron velocity is not reversed as it might be if the velocity would have been calculated in the drift approximation.

The space-charge distribution in the structure of the IW has three characteristic parts, the leading-edge distribution with a positive space charge, the solitary wave field with plasma oscillations within the region of rapid ionization, and the trailing edge with zero space charge. At the leading edge, a positive space charge is created due to ionization and acceleration of electrons in the cathode-directed external field, whose magnitude increases in the positive x direction. The space-charge distribution plays the key role in the process of the IW formation. When the electrons of an initial electron beam accelerate and ionize the neutral gas on their way they produce the positive space charge that is accumulated in the near-anode region. This space charge grows until its own electric field cancels the electric field at the anode. At that instant the maximum of the electric potential starts to propagate to the cathode and it is the beginning of the simultaneous propagation of both the IW and virtual anode. It should be noted that the distribution of the space charge is responsible also for the formation of fast IWs in weakly preionized plasma at lower values of E/N, for which the electron velocity can be calculated in the drift approximation. However, the condition of quasineutrality is fulfilled within the whole structure of such IWs [11], while for IWs in FCD a strong violation of quasineutrality occurs at the leading edge as is clearly seen in Fig. 10. A comparison of the absolute space-charge density (Fig. 7) and the parameter $\eta(\xi)$, which indicates the deviation from quasineutrality and represents the same difference normalized by the local concentration of ions $n_i(\xi)$ (Fig. 10), shows opposite trends in their behavior. At the leading edge, where the positive space-charge density is much less than the amplitude of the space-charge solitary wave, the quasineutrality condition is not fulfilled, while the large-amplitude solitary wave of the space charge is localized in the domain where $|\eta(\xi)| \ll 1$ and hence propagates in a quasineutral plasma.

It is worth noting that the solitary waves of the space charge, whose typical structure is shown in Fig. 7, differ from the classical Langmuir solitons in a collisionless plasma [31,32] in several respects. Unlike regular Langmuir solitons, for which plasma oscillations are localized in a domain with a reduced plasma density (sometimes such solitons are termed cavitons), the space-charge solitary waves associated with IWs exist in a partially ionized plasma, whose mean electron density increases across the ionization front. The increasing plasma density results also in an inhomogeneous filling of space-charge wave packets with oscillations since the plasma frequency increases across the IW. The regular Langmuir solitons are created due to modulation instability of plasmons and the balance of nonlinear self-constriction and dispersion. The solitary wave packets of space-charge oscillations associated with IWs are created by other mechanisms. The increase of the amplitude of space-charge oscillations occurs due to ionization growth at the leading edge of the IW, while the lowering of the amplitude at the trailing edge is provided by the relaxation of space charge in well-conducting plasma.

The calculated velocity of the IWs increases with the gas pressure (see Table I). This result agrees with experiment [17], in which the reduction of the time delay for electrical breakdown with the increase of the gas pressure was observed in a FCD. In the experiment [17] an alumina capillary with the inner radius $a = 0.4$ mm and the length $L = 1.5$ cm filled with argon was used. An electron beam originated in the HCR assisted the on-axis discharge initiation. The discharge operated at applied voltage 10–30 kV and the gas pressure in the HCR was 100–700 mTorr. The time delay for breakdown was determined as the length of time $\Delta t = t_2 - t_1$ between the first registration (at $t = t_1$) of the electron beam signal behind the anode measured by a Faraday cup and a scintillator-photomultiplier assembly and the instant t_2 when the total current began to increase rapidly. For the gas pressure in the HCR $p = 500$ mTorr the experimental time delay for breakdown was $\Delta t = 10$ ns. According to our estimate (see also Fig. 5 for the electric potential distribution), the time for the virtual anode formation is remarkably shorter than the time of its propagation from the anode to the cathode end of the capillary $t_W = L/W$. Therefore, we may compare the value of t_W calculated by our model of IW propa-

gation with the experimental time delay. First, it should be mentioned that the experimental time delay is weakly affected by the magnitude of applied voltage and this fact is in agreement with the weak theoretical dependence of the wave velocity on the virtual anode potential. The theoretical traverse time for $p=500$ mTorr is about 9 ns, which is close but less than the experimental time delay for breakdown. Even though the values of Δt and t_W have been found to be very close, it may only be concluded that the present model predicts reasonable order of magnitude for the time delay in the relevant range of parameters used in a FCD. This is due to the fact that some features of the experimental setup (such as variable radius of the shield and the axial pressure gradient in the capillary) cannot be reflected by steady-state solutions for IWs.

ACKNOWLEDGMENTS

The authors appreciate the support of this work by European Commission within the frame of the TMR Network Program under Contract No. ERBFMRX CT 98-0186.

[1] L. Loeb, Science **148**, 1417 (1965).
[2] W. P. Winn, J. Appl. Phys. **38**, 783 (1967).
[3] T. Suzuki, J. Appl. Phys. **48**, 5001 (1977).
[4] E. I. Asinovsky, A. N. Lagarkov, V. V. Markovets, and I. M. Rutkevich, Plasma Sources Sci. Technol. **3**, 556 (1994).
[5] L. M. Vasilyak, S. V. Kostyuchenko, N. N. Kudryavtsev, and I. V. Filyugin, Usp. Fiz. Nauk [Phys. Usp. **37**, 247 (1994)].
[6] J. Koppitz, J. Phys. D **6**, 1494 (1973).
[7] Yu. D. Korolev and G. A. Mesyats, *Physics of Pulse Breakdown in Gases* (Nauka, Moscow, 1990).
[8] K. H. Wagner, Z. Phys. **204**, 177 (1967).
[9] P. Strizke, I. Sander, and H. Raether, J. Phys. D **10**, 2285 (1977).
[10] A. J. Davies, IEE Proc., Part A: Phys. Sci., Meas. Instrum., Manage. Educ. **133**, 217 (1986).
[11] A. N. Lagarkov and I. M. Rutkevich, *Ionization Waves in Electrical Breakdown of Gases* (Springer-Verlag, New York, 1994).
[12] S. K. Dhali and P. F. Williams, J. Appl. Phys. **62**, 4696 (1987).
[13] C. Wu and E. E. Kunhardt, Phys. Rev. A **38**, 4396 (1988).
[14] K. Frank and J. Christiansen, IEEE Trans. Plasma Sci. **17**, 748 (1989).
[15] M. Favre, P. Choi, H. Chuaqui, Y. Kaufman, J. Moreno, E. Wyndham, and M. Zambra, IEEE Trans. Plasma Sci. **23**, 212 (1995).
[16] P. Choi, M. Favre, C. Dumitrescu-Zoita, J. Moreno, H. Chuaqui, and E. Wyndham, *Proceedings of the 4th International Conference on Dense Z-Pinches*, Vancouver, Canada, 1997, edited by N. R. Pereira, J. Davis, and P. E. Pulsifer, No. 409 (American Institute of Physics, New York, 1998) p. 353.
[17] M. Favre, H. Chuaqui, E. Wyndham, P. Choi, and C. Dumitrescu-Zoita, *40th Annual Meeting of the Division of Plasma Physics, New Orleans, 1998* [Bull. Am. Phys. Soc. **43**, R8S20 (1998)].
[18] K. Mittag, P. Choi, and Y. Kaufman, Nucl. Instrum. Methods Phys. Res. A **292**, 465 (1990).
[19] J. P. Boeuf and L. C. Pitchford, IEEE Trans. Plasma Sci. **19**, 286 (1991).
[20] A. V. Gurevich, Zh. Eksp. Teor. Fiz. **39**, 1296 (1961) [Sov. Phys. JETP **12**, 904 (1961)].
[21] F. J. de Heer, R. H. J. Jansen, and W. van der Kaay, J. Phys. B **12**, 979 (1979).
[22] G. Garcia, M. Roteta, F. Manero, F. Blanco, and A. Williart, J. Phys. B **32**, 1783 (1999).
[23] M. Mitchner and C. H. Kruger, Jr., *Partially Ionized Gases* (Wiley, New York, 1973).
[24] L. M. Biberman, V. S. Vorobjev, and I. T. Yakubov, *Kinetics of Non-Equilibrium, Low-Temperature Plasma* (Plenum, New York, 1986).
[25] B. L. Schram, Physica (Amsterdam) **32**, 197 (1966).
[26] D. E. Golden and H. W. Bandel, Phys. Rev. **149**, 58 (1966).
[27] N. F. Mott and H. S. W. Massey, *The Theory of Atomic Collisions* (Clarendon Press, Oxford, 1949).
[28] R. Courant and D. Hilbert, *Methods of Mathematical Physics, Vol. 2* (Interscience, New York, 1953).
[29] L. D. Landau and E. M. Lifshitz, *Fluid Mechanics* (Pergamon, New York, 1987).
[30] A. N. Lagarkov, S. E. Rasponomarev, and I. M. Rutkevich, Zh. Tekh. Fiz, **55**, 287 (1985) [Sov. Phys. Tech. Phys. **30**, 168 (1985)].
[31] A. A. Vedenov and L. I. Rudakov, Dokl. Akad. Nauk SSSR **159**, 766 (1964) [Sov. Phys. Dokl. **9**, 456 (1964)].
[32] V. E. Zakharov, Zh. Eksp. Teor. Fiz. **62**, 1745 (1972) [Sov. Phys. JETP **35**, 908 (1972)].